Theoretical study of terahertz generation from atoms and aligned molecules driven by two-color laser fields

Wenbo Chen, Yindong Huang, Chao Meng, Jinlei Liu, Zhaoyan Zhou, Dongwen Zhang, Jianmin Yuan, and Zengxiu Zhao*

Collage of Science, National University of Defense Technology, Changsha 410073, People's Republic of China

(Received 29 March 2015; published 9 September 2015)

We study the generation of terahertz radiation from atoms and molecules driven by an ultrashort fundamental laser and its second-harmonic field by solving the time-dependent Schrödinger equation (TDSE). The comparisons between one-, two-, and three-dimensional TDSE numerical simulations show that the initial ionized wave packet and its subsequent acceleration in the laser field and rescattering with long-range Coulomb potential play key roles. We also present the dependence of the optimum phase delay and yield of terahertz radiation on the laser intensity, wavelength, duration, and ratio of two-color laser components. Terahertz wave generation from model hydrogen molecules is further investigated by comparing with high harmonic emission. It is found that the terahertz yield follows the alignment dependence of the ionization rate, while the optimal two-color phase delays vary by a small amount when the alignment angle changes from 0 to 90 degrees, which reflects the alignment dependence of attosecond electron dynamics. Finally, we show that terahertz emission might be used to clarify the origin of interference in high harmonic generation from aligned molecules by coincidentally measuring the alignment-dependent THz yields.

DOI: 10.1103/PhysRevA.92.033410 PACS number(s): 33.20.Xx, 42.50.Gy, 42.65.Ky

I. INTRODUCTION

Terahertz (THz) radiation, with wavelength between 0.03 to 3 millimeters, has been found useful for applications in information and communication technology, homeland security, global environmental monitoring, and ultrafast computing, to name a few [1,2]. Scientifically, it provides resonant access into, and hence enables the probing of, various modes, such as the motion of free electrons, the rotation of molecules, the vibration of crystal lattices, and the precessing of spins [3]. With power continually being increased and duration being shortened into a single or half cycle, pulsed intense THz sources are now capable of driving and steering nonresonant ultrafast processes in matter in unique ways. New phenomena are being observed, e.g., THz harmonic generation [4], strong-field control of spin excitation [5] and phase transition [6], etc.

The efficient generation of a THz wave, however, is still challenging. The popular approaches include optical THz generation, solid-state electronics, and quantum cascade laser, which are limited either by low-frequency conversion efficiency, low-temperature requirement, or the lack of eigenoscillator [7]. Among these techniques, laser air photonics is capable of generating THz field strength greater than 1 MV/cm with bandwidth of over 100 THz through plasma formation by a laser-ionized gaseous medium [8]. But the mechanism of THz generation from the laser-induced plasma turns out be complicated [9] and involves wave propagation, plasma formation, oscillation, and collision. For example, the THz can be emitted by the radical acceleration of the ionized electrons due to the ponderomotive force generated by the radial intensity gradient of the optical beam [10], by linear mode conversion from the laser-induced plasma wake field in an inhomogeneous plasma [11,12], or by a Cerenkov-type mechanism from light propagating within the filament [13].

In this work, we restrict our study to a single-atom or -molecule response by focusing on THz generation from gases of much lower densities in low pressure and minimizing the collective motion of plasma and its modification on the light propagation. Even in this much simpler case, the mechanism of THz emission is still under debate, partly because of the involved complex dynamics during laser interaction with gases. Nevertheless, down to the fundamental origin of THz emission, it could only either be the induced current or the induced polarization. Therefore, two popular mechanisms are proposed, i.e., a microscopic photocurrent (PC) model with tunneling photoionization [14,15] and a third-order nonlinear model with four-wave mixing (FWM) [16–18].

Both models qualitatively agree with the experimental findings that the broken symmetry of the laser-gas interaction could enhance the field strength of the emitted THz waves by several orders of magnitude, when either applying a dc bias [19,20], an ac bias by using two-color pulses [16] or using a carrier-envelope phase stabilized few-cycle pulse [21]. As a representative case, THz emission in two-color laser fields has been investigated more intensively [14–17,21–29]. So far, more evidence supports the model based on the photocurrent as it is found that ionization is indispensable [16], although the physics behind photocurrent formation needs to be explored carefully [30]. However, in view of the success of the four-wave mixing model applied to the THz detection through an air-breakdown coherent detection scheme [18,31], the two models must be closely connected.

The full quantum description in our previous work and others [30,32–35] provides more insight into the mechanism of THz emission. By connecting THz emission with high harmonic generation (HHG) in two-color laser pulses, the dynamics responsible for THz emission is attributed to the continuum-continuum transition during laser-assisted soft collision of the ionized electron with the atomic core, while the hard collision with the atomic core leads to HHG upon recombination [30,31].

*zhao.zengxiu@gmail.com

Because the fundamental pulse is strong enough to induce ionization, its interaction with the gas cannot be treated perturbatively. The interaction with the second-harmonic pulse is, however, weak, which seems to be possibly treated perturbatively on top of the nonperturbative behavior from the fundamental pulse. In this sense, the photocurrent model can be understood by another type of four-wave mixing model, but different from the usual case in which the involved lower and upper states could really be populated by multiphoton ionization or tunneling ionization. Therefore, the two models can be unified, as hinted in Refs. [9,30–32,35].

Although the second-harmonic pulse is very weak, it serves as a gate controlling the phase of the electron wave packet and hence breaks the left to right symmetry leading to the formation of net current and the emission of THz waves. At the same time, the out-of-phase high harmonic emission between the adjacent half cycle in the single-color pulse is changed as well, leading to the emission of even-order high harmonics [36–40]. Therefore, by controlling the phase delay between the fundamental and the second-harmonic pulse, the THz and high harmonic yield can be controlled simultaneously. This enables the calibration of the optimal phase delay (OPD) maximum THz yields and it is found that the OPDs are related to the atomic potential [30,31]. It is thus expected that the sensitivity of THz yields to the Coulomb potential might be used to map atomic fields from within and to help the full characterization of the rescattering wave packet [30].

In the present investigation, we explore further the effects of atomic potential and other laser parameters on the generation of THz for both a hydrogen atom and a model H_2^+ molecule interacting with two-color pulses. It is known that the structure and alignment of molecules can be revealed from HHG [41,42]. But how these affect THz generation has been unclear. The findings in this work include the following: (1) The alignment of molecules and the geometry of molecular orbital affect the yields of THz generation; (2) the optimal phase of THz generation from two-color pulses shows weak dependence on the molecular alignment, reflecting the attosecond electron dynamics in the alignment-dependent molecular potential; (3) scaling of THz yields with driving laser frequency; and (4) the connection of THz generation and HHG at different alignment. These findings are crucial for better tomography imaging of the molecular orbital because both the ionization rate and the HHG yield can be measured simultaneously. Although both radiations are measured in far field, it is shown that THz can be used as a coherent counterpart of harmonics in the investigation of near-field electron dynamics and molecular structures.

The paper is organized as follows. In Sec. II, we present the theory and model for THz generation from ionizing atoms by two-color laser pulses. In Sec. III, we show the calculated results and discuss the underlying physics. Finally, we draw conclusions in Sec. IV.

II. THEORY AND METHODS

A. Photocurrent model

Under strong laser fields, the electron current is presumably contributed by photoelectrons released after ionization [15]. When the laser photon energy is much less than the ionization potential I_p, and $I_p < 2U_p$ where the ponderomotive energy U_p is the averaged kinetic energy of an electron moving in the laser field, the mechanism of ionization can be considered as tunneling of the electron through the potential barrier formed by the atomic potential and the instantaneous electric dipole potential. The instant ionization rate in the electric field of $E(t)$ can be obtained using the Ammosov-Delone-Krainov (ADK) model [43,44],

$$w(t) = I_p |C_{n^*}|^2 \left\{ \frac{2\kappa^3}{|E(t)|} \right\}^{2n^*-1} \exp\left\{ -\frac{2\kappa^3}{3|E(t)|} \right\}, \quad (1)$$

where Z_c and I_p are the net resulting charge and ionization potential of the atom, respectively, and $I_{\rm ph} = 0.5$ a.u. is the ionization potential of the hydrogen atom. Also, $\kappa = \sqrt{2I_p}$, $n^* = Z_c\sqrt{I_{\rm ph}/I_p}$, and $C_{n^*} = \frac{2^{2n^*}}{n^*\Gamma(n^*+1)\Gamma(n^*)}$.

If the laser field strength is much higher such that the binding energy of the electron is higher than the height of the potential barrier, ionization can proceed through over-the-barrier ionization (OTBI). In the OTBI range, we can use the following empirical formula suggested by [45]:

$$w_{\rm OTBI}(t) = w_{\rm TI}(t) e^{-\alpha(Z_c^2/I_p)(E(t)/\kappa^3)}. \quad (2)$$

Once the instantaneous ionization rate is found, the free electron density as a function of time can be obtained by

$$n_e(t) = n_0 \left\{ 1 - \exp\left[-\int_{-\infty}^{t} w(t')dt' \right] \right\}, \quad (3)$$

where n_0 is the neutral atom density. Assuming the subsequent motion of the electron after ionization is dominated by the laser field, the photon current and its acceleration contributed by the ionization event t_i are

$$j(t_i,t) = -n_0(t_i) w(t_i) \left[p(t_i) + \int_{t_i}^{t} E(t')dt' \right], \quad (4)$$

$$a(t_i,t) = -n_0(t_i)\, w(t_i) E(t). \quad (5)$$

Note that we take the initial longitudinal momentum $p(t_i) = 0$ at the instant ionization. The total photon current $J(t)$ and dipole acceleration $A(t)$ are thus formulated as

$$J(t) = \int_{-\infty}^{t} j(t_i,t)dt_i, \quad (6)$$

$$A(t) = \int_{-\infty}^{t} a(t_i,t)dt_i. \quad (7)$$

From the current, the net residual current density (RCD) after the pulse is given by $J_{\rm RCD} = J(t \to \infty)$. The frequency-domain spectrum $F(\Omega)$ is calculated by the Fourier transformation of acceleration $A(t)$ with intensity given by $G(\Omega) = |F(\Omega)|^2$. The total yields of THz radiation is given by the integral of the spectra intensity from 0 up to 30 THz.

B. Time-dependent Schrödinger equation

The time-dependent Schrödinger equation (TDSE) for an atom interaction with the laser field in dipole approximation

is given by

$$i\frac{\partial}{\partial t}\Psi(\mathbf{r},t)=\left[\frac{\hat{\mathbf{p}}^2}{2}+\hat{V}(r)+\mathbf{r}\cdot\mathbf{E}(t)\right]\Psi(\mathbf{r},t), \quad (8)$$

where the linearly polarized (along the $\hat{z}$ direction) two-color laser field is given by

$$\mathbf{E}(t)=[E_\omega\cos(\omega t)+E_{2\omega}\cos(2\omega t+\phi)]\hat{z}f(t). \quad (9)$$

Here, E_ω, $E_{2\omega}$, $f(t)$, ω, and ϕ denote the fundamental and its second-harmonic laser field strength, temporal envelope, fundamental frequency, and two-color phase delay, respectively. By numerically solving the TDSE in three dimensions, the induced dipole acceleration along the $\hat{z}$ direction is given by the quantum average,

$$a(t)=\left\langle\frac{\partial V}{\partial z}-E(t)\right\rangle, \quad (10)$$

from which the THz radiation can be obtained by Fourier transformation. The corresponding electron current density [46] is given by $J(t)=\int_{-\infty}^{t}a(t)dt$ and can be recast into

$$J(t)=J'(t)+J_{bb}(t),$$

where the fast oscillation part $J_{bb}(t)$ results from the dipole transitions between the populated Rydberg states, and $J'(t)$ is the rest part of the current, which generates the broadband terahertz radiation. The residual current density can be found numerically by time averaging the current after the laser turns off to cancel the $J_{bb}(t)$ component, $J_{\mathrm{RCD}}=\frac{1}{\tau}\int_{t_f}^{t_f+\tau}dt\,J(t)$, which can be directly compared to that from the PC model. The THz spectra and yields can be computed from the dipole acceleration in the same manner given in the previous section.

As an example, we show in Fig. 1 the typical THz yield modulations from a hydrogen atom in the two-color laser pulse, obtained from the TDSE simulation. As the two-color phase delay varies, the modulations of terahertz yield below 10 THz, 30 THz, and RCD take the maximum at nearly the same optimum phase delay (OPD) ϕ_m, as shown in Fig. 1. It suggests that the RCD can be used as a good parameter characterizing the phase-delay dependence of THz yields. On the other hand, the ionization probability is less modulated by the applied weak second-harmonic pulse, which indicates that the modulation of THz yield is mainly contributed by the controlling of the electron dynamics after ionization, in accordance with the analysis presented in [30,31]. For comparison, we show the modulation of RCD from the PC model, which deviates from the TDSE calculation because of the neglecting of the Coulomb potential in the dynamics of free electrons.

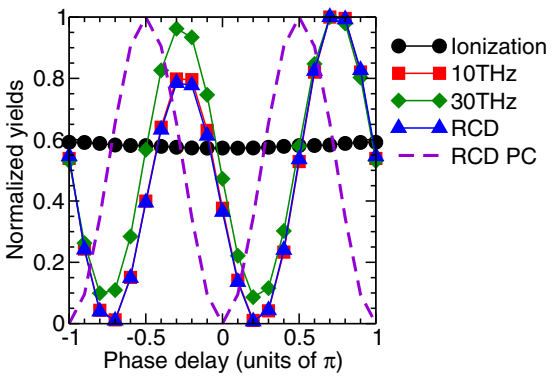

FIG. 1. (Color online) Modulation of THz yields below 10 THz (red square) and 30 THz (green diamond), residual current density (blue triangle) and ionization probability (black circle) from TDSE simulations, and RCD from the PC model (violet dashed line) as functions of the phase delay between the two-color pulses. The TDSE and PC calculations are carried out for hydrogen atoms. The fundamental laser pulse has the intensity of 2×10^{14} W/cm^2, wavelength of 800 nm, FWHM of 25 fs, and the second-harmonic intensity is 1% of fundamental pulse.

III. RESULTS AND DISCUSSIONS

A. Atomic terahertz generation: Laser intensity and wavelength

We first examine in detail how the THz yields from hydrogen atoms depend on various parameters of the two-color laser pulses; we especially pay attention to the optimal phase delay that maximizes the THz yields. In Fig. 2, the laser-intensity dependence of the optimal phases and the corresponding THz yields are compared between different models. The ionization potential is adjusted, taking the same value of $I_p=0.5$ a.u. When the atomic potential is the long-range Coulomb potential, for either one-dimensional (1D), 2D, or 3D calculations, the optimal phase follows the same trend that changes from 0.9π to 0.6π as the laser intensity varies from I_0 to $10I_0$, where $I_0=10^{14}$ W/cm^2. In contrast, the optimal phase predicted by the PC model varies little around 0.5π (the variation might be due to the depletion of the ground state). It confirms our previous investigation that the PC model for THz generation fails due to the ignorance of the Coulomb potential [30]. When a short-range potential rather than the Coulomb potential is used, such as for the negative ions, the optimal phase of THz generation shows completely different behavior, increasing from 0.1π to 0.5π as the laser intensity increases, as shown in Fig. 2(a). It clearly demonstrates the importance of the long-range potential.

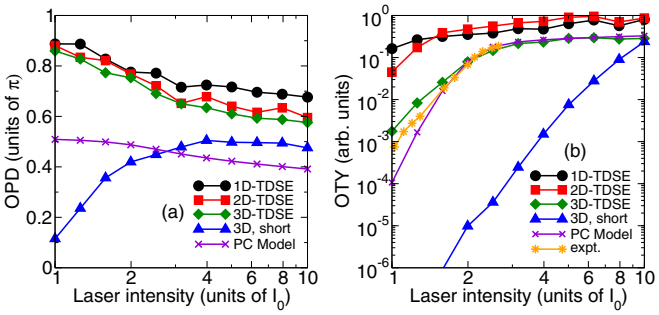

FIG. 2. (Color online) The (a) optimal yields and (b) corresponding optimal phase delay of THz generation at various laser intensities calculated by 1D (black circles), 2D (red squares), and 3D (green diamonds) TDSE with Coulomb potential, 3D-TDSE short-range potential. The laser intensity is in units of I_0 with $I_0=1\times10^{14}$ W/cm^2, and the ionization potential is $I_p=0.5$ atomic units for all cases. The experimental data (orange stars) are taken from [15].

The variation of the OPD with laser intensity indicates that different ionization mechanism are involved. Let us now focus on the optimal phases from the 3D calculations with Coulomb potentials that are closely related to the experimental observation. As the laser intensity increases, the ionization mechanisms change from multiphoton ionization (MPI) to tunneling ionization (TI), and then over-the-barrier ionization (OTBI).

In the regime of MPI when $\gamma > 1$, terahertz generation is dominated by four-wave mixing [32] with prediction of the terahertz field strength given by $E_{\mathrm{THz}}(t) \propto \chi^{(3)} E_{2\omega}(t) E^*_{\omega}(t) E^*_{\omega}(t) \cos\phi$ and the OPD is close to 0 or π, in agreement with the numerical results at the laser intensity of $I_0 = 10^{14}$ W/cm^2. When TI dominates ($\gamma < 1$), the soft recollision between the ionized electron with the atomic core's Coulomb potential plays the key role [30,31]. Rescattering currents dominate and escaped currents vanish, and the OPD shifts from π to 0.6π. With further increasing of the laser intensity, OTBI takes over for laser intensity over $I = \frac{\kappa^4}{16 I_p}$. The nonvanishing initial longitudinal momentum causes the enhancing of the escaped part of the electron wave packet, and hence the OPD is close to 0.5π. In this case, the atomic potential might be neglected and hence the photon-current model holds, predicting the terahertz field as $E_{\mathrm{THz}}(t) \propto dJ(t)/dt \propto f[E_\omega(t)] E_{2\omega}(t) \sin\phi$.

We now turn to the dependence of optimal terahertz yields (OTYs) on the laser intensity. Due to the absence of hydrogen experimental THz data, we compare our simulation with the experiments [15] by linearly scaling the total input pump energy to laser intensity and choosing the maximal intensity as the saturation intensity of the argon atom. Surprisingly, the 3D calculation, the photocurrent model, and the experimental data [15] give quite similar dependence. It indicates that the ionization rate is crucial in determining the yields, since the ADK ionization rate is derived for a 3D hydrogen atom. In contrast, the 1D and 2D calculations overestimate the ionization yield because the wave packet is less spreading compared to the 3D case. It is also worth noting that the yields from the short-range potential are much lower for two reasons. First, the tunneling ionization rate at the same ionization energy is indeed smaller for the short-range potential compared to the long-range potential. Second, the laser-assisted soft collision is suppressed in the case of short-range potential.

Next, we examine how the optimal phase delay and yields depend on the intensity ratio, $\alpha = I_{2\omega}/I_\omega = E^2_{2\omega}/E^2_\omega$, between the second-harmonic and fundamental pulse. As shown in Fig. 3(a), the optimal phase delay remains nearly constant for $\alpha < 0.1$ for the given fundamental laser intensity ($I_\omega = 1.5 \times 10^{14}$ W/cm^2) of the fundamental pulse. But as the intensity ratio increases further, the OPD quickly drops to 0.5π because the second-harmonic pulse begins to participate in the ionization process, which eventually take over the ionization from the fundamental pulse. It is shown in Fig. 3(b) that the OTYs are scaled as a power of the intensity ratio, which is consistent with the experiment [47]. The dependence on the intensity ratio of both the OPD and OTY is consistent with the laser-assisted soft-collision model presented in [31]. For convenience of direct comparison to experiments, we present

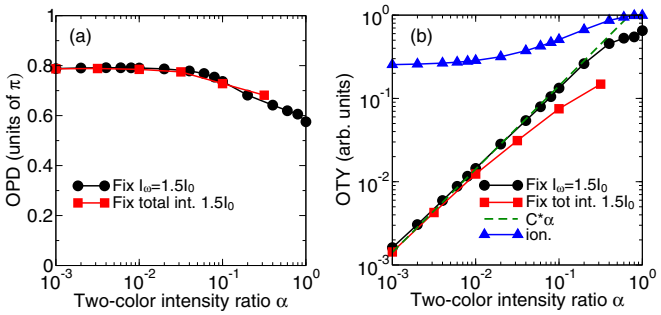

FIG. 3. (Color online) The scaling of (a) OPD and (b) OTY of THz generation with the intensity ratio of the second-harmonic pulse to the fundamental laser pulse. The peak pump intensity of the fundamental (black circles) or total (red squares) laser pulse is fixed at $1.5I_0$. The blue square line denotes the ionization population and the green dashed line is scaled as the power of the intensity ratio.

the intensity-ratio dependence by fixing the total power of the fundamental and the second-harmonic pulse, and the similar conclusion can be drawn as well. The ionization probability is also shown in Fig. 3(b), which is less dependent on the intensity ratio, suggesting the dynamics following ionization is crucial in terahertz wave generation.

To further clarify the mechanism of THz wave generation by two-color laser pulses, we examine the wavelength scaling of THz generation. As the wavelength increases, the OPDs obtained from TDSE shift from 0.8π to 0.5π, as shown in Fig. 4(a), while the PC model predicts the OPD at 0.5π independent of wavelength. The variation of OPDs with wavelength might be rationalized as follows. Because the wave packet is more diffused during each cycle for the longer wavelength, the soft recollision with the atomic nucleus plays less of a role, resulting in the OPD at 0.5π as predicted by the PC model, which neglects the Coulomb potential completely.

On the other hand, according to the PC model, the OTYs are scaled quadratically with the wavelength, while the TDSE simulation shows deviation from this dependence. As shown in Fig. 4(b), the OTYs from the TDSE calculation are scaled as $\lambda^{1.45}$, at the laser intensity of $I_\omega = 2I_0$, while for $I_\omega = 1.5I_0$

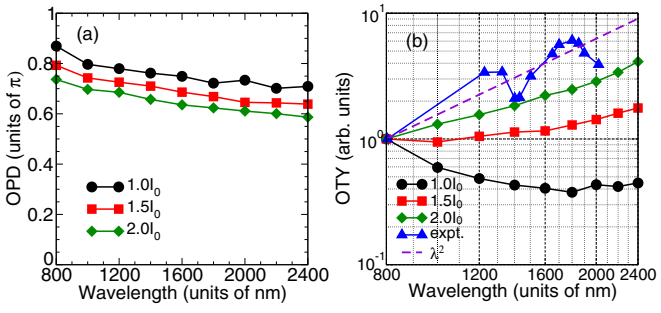

FIG. 4. (Color online) Wavelength scaling of (a) the optimum phase delay and (b) THz yields. The experimental data is taken from [48]. The fundamental laser intensities equal to I_0 (black circles), $1.5I_0$ (red squares), and $2I_0$ (green diamonds), respectively. Here, the two-color intensity ratio $\alpha = 1\%$ and the laser pulse has duration of FWHM 50 fs.

or I_0, the deviation is even bigger. One of the reasons for the deviation is the diffusion of the electron wave packet. However, the experimental data from Clerici *et al.* [48] is closer to the prediction of the PC model. This discrepancy needs further investigation in the future. Note that the experimental data show oscillations as varying the driving wavelength. Because both the focal length and the input energy are fixed in the experiment, we suspect that the peak pump intensity, the two-color intensity ratio, and the phase delay might be varying in the focusing volume as a result of the focusing geometry. In particular, THz yield is sensitive to the two-color intensity ratio and its fluctuations could cause the oscillation of THz yields when the laser wavelength is changing.

B. Terahertz wave generation from aligned molecules

The previous investigation of THz generation from atoms in two-color laser fields demonstrates the importance of Coulomb potential on the laser-driven electron dynamics. In addition, it confirms the sensitivity of THz yields on the detuning of ionization and electron dynamics. For molecules, it is therefore expected that THz generation might exhibit dependence on both molecular alignment and molecular orbital.

To simulate molecular terahertz generation, we numerically solve the two-dimensional TDSE for a model H_2^+ with the soft-core potential between the electron and the two nuclei,

$$V(\mathbf{r}) = -\frac{Z_c}{\sqrt{(\mathbf{r}-\mathbf{R}/2)^2+a^2}} - \frac{Z_c}{\sqrt{(\mathbf{r}+\mathbf{R}/2)^2+a^2}} - Z_s e^{-[(\mathbf{r}-\mathbf{R}/2)/r_s]^2} - Z_s e^{-[(\mathbf{r}+\mathbf{R}/2)/r_s]^2}, \quad (11)$$

where $\mathbf{r} = (z,x)$ and $\mathbf{R} = (R\cos\theta, R\sin\theta)$ are the electronic and molecular coordinates, and R is the internuclear distance. The two-color pulse is used. The fundamental and the second-harmonic pulses are chosen parallel in polarization along the $\hat{z}$ axis. θ is the alignment angle between the molecular axis and the laser polarization $\hat{z}$, a is the soft-core parameter, and Z_c is the effective charge of each nuclei. The last two terms in $V(\mathbf{r})$ are the additional short-range potential to adjust the ionization energy. Here, the motion of the nuclei is frozen and we set $Z_c = 1$ a.u., $R = 2$ a.u., $a = 1$ a.u., $Z_s = 0$, and the ionization energy I_p is equal to 0.934 a.u.

The emitted THz radiation is calculated from the low-frequency part of the Fourier transformation of the induced dipole moments both parallel and perpendicular to the laser polarization. The total terahertz yield is the sum of the yield of the parallel $G_\parallel$ and perpendicular $G_\perp$ direction. As shown in Fig. 5(a), when the laser intensity is in the tunneling regime ($\gamma > 1$ and $I > 2.1 \times 10^{14}$ W/cm^2), the OTY of the terahertz field parallel to the laser polarization is two orders larger than that from the perpendicular direction for molecules aligned at 45° with respect to the laser polarization. At 0° and 90° alignment, the perpendicular components vanish. Therefore, the total THz yields are dominated by the emission of the THz wave with the field component parallel to the laser polarization and, in the following, we do not distinguish between the total yield and the yield parallel to the laser polarization. Figure 5(b) shows the OPDs of THz for molecules at different alignment.

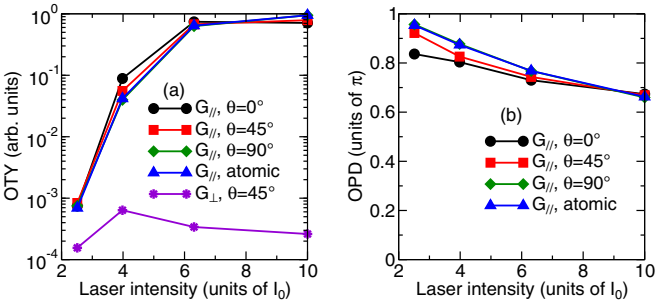

FIG. 5. (Color online) Comparison of (a) the OTY and (b) the OPD of THz generation from molecules at alignment angle $\theta = 0°$ (black circles), 45° (red squares), 90° (green diamonds), and from atoms (blue triangles). Here, $\parallel$ and $\perp$ denote the THz yields that are parallel and perpendicular to the laser polarization, respectively.

The OPD varies from π in the MPI range to 0.6π in the TI or OTBI range as the laser intensity increases, similar to the case of atoms.

For a given two-color laser intensity, e.g., $I_\omega = 4 \times 10^{14}$ W/cm^2, $I_{2\omega} = 0.5\% I_\omega$, we examine in detail how the OTYs vary with alignment angle. Figure 6(a) shows that the total OTYs take maximum at $\theta = 0°$ and minimum at $\theta = 90°$, respectively, which closely resembles the angular dependence of the ionization probability [49,50]. However, the perpendicular component of the THz wave, although much weaker, exhibits very different alignment dependence, reaching a maximum at $\theta = 45°$ in contrast to the parallel component.

We now investigate the alignment dependence of the OPDs. As shown in Fig. 6(b), the OPDs of the total THz wave yields (mainly the parallel component) vary with the alignment angle θ. The maximum variation $\Delta\phi_m = \phi_m(\theta) - \phi_m(0)$ is found less than 0.1π. Although the variation is small, it indeed indicates that the molecular potential plays a role in the generation of THz waves. In fact, converted into a time scale, the phase change of 0.1π corresponds to a time delay of 67 attoseconds (as). For a better illustration, the variations $\Delta\phi_m$ are plotted for both the parallel and perpendicular components in Fig. 6(c). For both components, it can be seen that the OPD increases as the alignment angle increases and reaches a maximum at 90° alignment. The extra phase delay for molecules perpendicular to the laser polarization

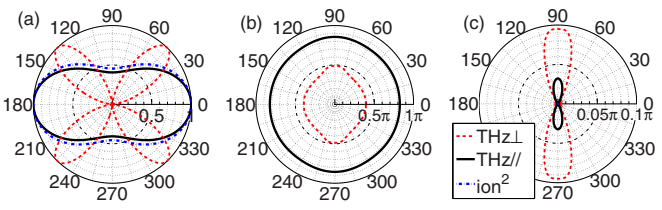

FIG. 6. (Color online) Alignment-resolved OPD and OTY for THz generation from H_2^+. (a) Normalized OTY parallel (black solid line) and perpendicular (red dashed line) to laser polarization, and normalized ionization population (blue dash-dotted line). (b) OPD. (c) OPD difference at various alignment angles to that of $\theta = 0°$. The laser pulse parameters are $\omega = 0.057$ a.u., $I_\omega = 4I_0$, $I_{2\omega} = 0.5\% I_\omega$, and FWHM = 15 fs.

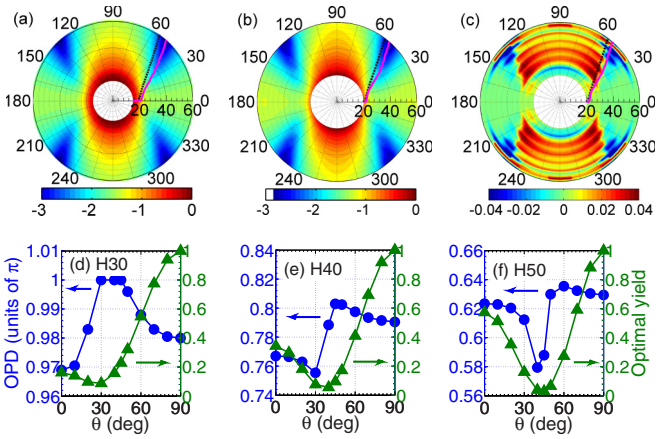

FIG. 7. (Color online) Harmonic generation from H_2^+. (a) Odd-harmonic yields in one-color laser. (b) Even-harmonic yields from the two-color laser pulse. (c) OPD difference of even harmonics relative to $\theta = 0^\circ$. (d)–(f) The OPDs (blue circles) and optimum yields (green triangles) of the 30th, 40th, and 50th harmonics, respectively, as functions of alignment angles θ.

might be attributed to the larger recollision cross section in this geometry, which leads to a larger distortion of the electron trajectories and hence more pronounced focusing effects during THz wave emission.

In order to provide more insight into the generation of terahertz waves from molecules, we present the results of high harmonic generation (HHG) as well. In Fig. 7(b), the optimal yields of even harmonics from the two-color laser pulse are shown in a contour plot against the alignment angles. For comparison, high harmonic yields from the fundamental pulse alone are presented in Fig. 7(a). It can be seen that the yields of even harmonics generated by the two-color laser field peak at both alignments of 0° and 90°, which resembles the behavior of odd harmonics generated by the one-color laser pulse. However, this is in stark contrast to the alignment dependence of terahertz radiation yields, which peak at zero alignment [see Fig. 6(a)]. It is worth noting that the minimum of harmonic yields [shown in red lines in Figs. 7(a) and 7(b)] are in accordance with the prediction (shown in black lines) that the destructive two-center interference occurs for $R\cos\theta = (2m+1)\lambda/2$, $m = 0,1,\ldots$, where λ is the electron wavelength and the electron energy is determined by $E_k = N\omega$ [51].

By varying the phase delay between the two pulses, both even-harmonic and terahertz wave yields modulate. In Figs. 7(d)–7(f), we show the OPD and OTY for 30th, 40th, and 50th harmonics as functions of alignment, respectively. It can be seen, wherever the OTY takes the minimum, that the corresponding OPD makes a phase jump. In contrast, the OPD of the THz wave shows a slow variation with the molecular alignment [see Fig. 6(b)]. As mentioned above, THz and HHG radiate from a laser-assisted soft and hard collision of the ionized electron with the atomic or molecular core, respectively. The terahertz generation is insensitive with the ion potential and its yield is dominated by the ionization rate at different alignment angles for given laser parameters. Therefore, the OPD and OTY of THz shows a smooth

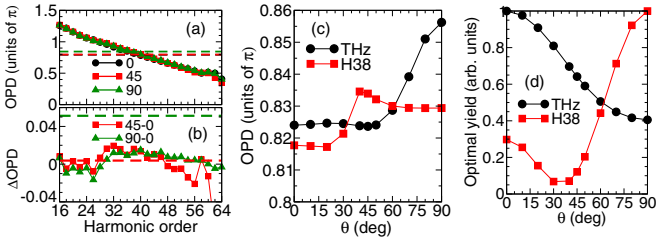

FIG. 8. (Color online) (a) The OPD of HHG at alignment angles θ of 0° (black circles), 45° (red squares), and 90° (green triangles). The black, red, and green dashed lines denote the OPDs of terahertz waves at the corresponding angles. (b) The OPD difference of HHG at 45° and 90° with respect to the alignment of 0° angle. The alignment-dependent (c) OPDs and (d) optimum yields of THz (black circles) and the 38th-harmonic (red squares) generation by the two-color laser pulse.

variation with θ. On the other hand, HHG is very sensitive to the recombination dipole moments, which can be viewed as the quantum interference of the emissions from the two atomic centers. In particular, when the HHG yield takes a minimum, there is a phase jump of the recombination dipole moments. Because the even harmonics is closely related to the neighboring odd harmonics, its modulation with the two-color phase delay shows a phase jump at the minimum related to the phase difference of the recombination dipole moment across the minimum.

For alignment of 0°, 45°, and 90°, the OPDs as functions of the harmonic order are shown in Fig. 8(a). It can be seen in all three cases that the OPD is nearly linear with respect to the harmonic order, reflecting the chirp of the recombined electron wave packet during HHG processes [52]. Detailed examination of Fig. 8(b) shows that the OPD for alignments 45° and 90° differs slightly from that of 0° alignment.

To make more close contact of THz and HHG, the OPD and OTY of the 38th-harmonic yields are shown in comparison with terahertz generation in Figs. 8(c) and 8(d). It clearly demonstrates that THz yields can be used to gauge the harmonic yield to gain the two-center interference information of HHG. The phase-delay dependence of THz generation can be used to probe the modulation of harmonics as well.

In order to better understand the terahertz generation dependence on the molecular orbital, we further simulate the angular-resolved THz yield of various molecular potential, with parameters given in Table I. The molecular orbital wave functions and terahertz yields are shown in Fig. 9. The phase delays between the two-color pulses are fixed at 0.8π, and the peak pump intensities are $I_\omega = 4I_0$ for V_1, $1.5I_0$ for V_2,

TABLE I. The parameters of various molecular potential.

Potential	R	Z_c	a	Z_s	r_s	Orbital	I_p (eV)
V_1	2	1.0	1.0	0		$1s\sigma_g$	25.41
V_2	2	0.5	0.5	1.17	1	$2p\sigma_u$	15.59
V_3	2	0.5	0.5	3.93	1	$3p\pi_u$	12.03

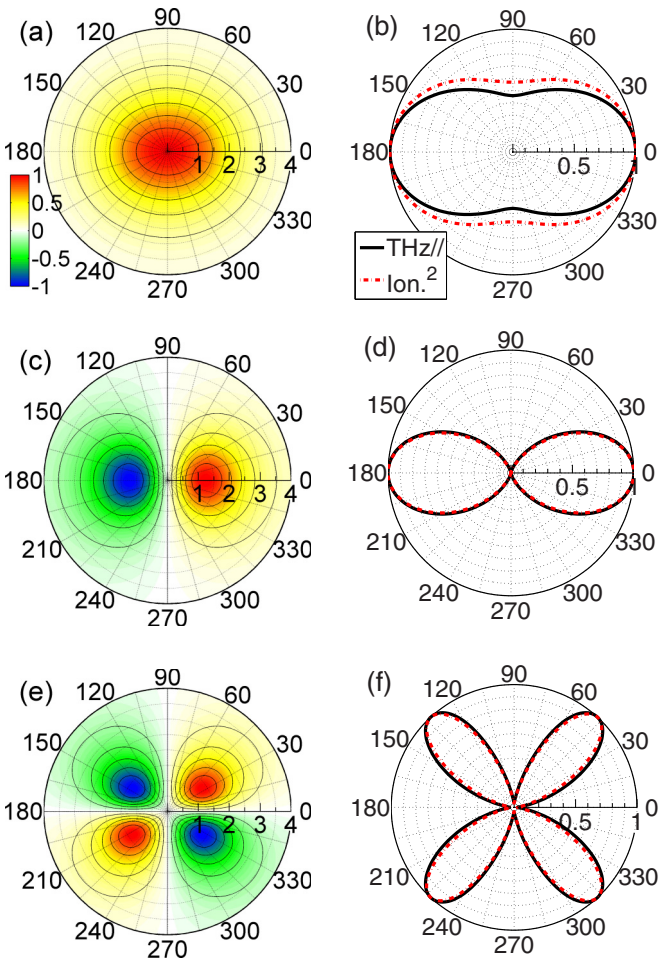

FIG. 9. (Color online) (a),(c),(e) The molecular orbital wave functions of potentials V_1, V_2, and V_3, respectively, with parameters given in Table I. (b),(d),(f) The corresponding alignment-resolved terahertz yield (black line) and squared ionization population (red dashed line) driven by the two-color laser pulse. The laser parameters are $I_\omega = 4I_0$ for V_1, $1.5I_0$ for V_2, $0.8I_0$ for V_3, and $\omega = 0.057$ a.u., $I_{2\omega} = 1\%I_\omega$, two-color phase delay $\phi = 0.8\pi$, trapezoidal envelope with one-cycle turn-on, six-cycle plateau, and one-cycle turn-off.

and $0.8I_0$ for V_3, respectively. For comparison, the THz yields from H_2^+ are shown again, the same as in Fig. 6(a). It can be seen for both molecular orbitals $2p\sigma_u$ and $3p\pi_u$ that the alignment-dependent THz yields follow almost exactly the square of the ionization rates. We therefore confirm that THz yields can be used to calibrate the alignment dependence of the ionization rate.

IV. CONCLUSIONS

In conclusion, we have investigated the atomic and molecular terahertz generation with intense two-color laser pulses. Based on the TDSE simulation, we show that THz generations are dominated by the competition between the laser field and the long-range Coulomb field, which can affect the ionization mechanism and wave-packet dynamics. As the laser intensity increases, the OPD variations demonstrate that the dominating mechanisms of THz generation are changing from four-wave mixing, rescattering currents of soft recollision between the ionized electron with the atomic core, to the photocurrent model without Coulomb potential. When we focus on THz generation dependence on both the molecular alignment angle and molecular potential, the total OTY is closely similar to the angular dependence of the ionization probability, and the OPD variation of several tens of attoseconds indicates that the molecular potential plays a role in the generation of THz waves. Finally, we show that both the alignment dependence of the OTY and OPD of THz generation can be used to contrast with that of high harmonic generation, which might be used to further explore the corresponding attosecond electron dynamics experimentally.

ACKNOWLEDGMENTS

This work is supported by the National Basic Research Program of China (973 Program) under Grant No. 2013CB922203, and the National Natural Science Foundation of China (Grants No. 11374366 and No. 11274383).

[1] M. Tonouchi, Nat. Photon. **1**, 97 (2007).
[2] M. C. Hoffmann and J. A. Fülöp, J. Phys. D: Appl. Phys. **44**, 083001 (2007).
[3] T. Kampfrath, K. Tanaka, and K. A. Nelson, Nat. Photon. **7**, 680 (2013).
[4] B. Zaks, R. B. Liu, and M. S. Sherwin, Nature (London) **483**, 580 (2012).
[5] T. Kampfrath, A. Sell, G. Klatt, A. Pashkin, S. Mährlein, T. Dekorsy, M. Wolf, M. Fiebig, A. Leitenstorfer, and R. Huber, Nat. Photon. **5**, 31 (2011).
[6] M. Liu, H. Y. Hwang, H. Tao, A. C. Strikwerda, K. Fan, G. R. Keiser, A. J. Sternbach, K. G. West, S. Kittiwatanakul, J. Lu, S. A. Wolf, F. G. Omenetto, X. Zhang, K. A. Nelson, and R. D. Averitt, Nature (London) **487**, 345 (2012).
[7] D. Saeedkia and S. Safavi-Naeini, J. Lightwave Technol. **26**, 2409 (2008).
[8] B. Clough, J. Dai, and X.-C. Zhang, Mater. Today **15**, 50 (2012).
[9] M. D. Thomson, M. Kress, T. Löffler, and H. G. Roskos, Laser Photon. Rev. **1**, 349 (2007).
[10] H. Hamster, A. Sullivan, S. Gordon, W. White, and R. W. Falcone, Phys. Rev. Lett. **71**, 2725 (1993).
[11] Z.-M. Sheng, H.-C. Wu, K. Li, and J. Zhang, Phys. Rev. E **69**, 025401 (2004).
[12] Z.-M. Sheng, K. Mima, J. Zhang, and H. Sanuki, Phys. Rev. Lett. **94**, 095003 (2005).
[13] C. D'Amico, A. Houard, M. Franco, B. Prade, A. Mysyrowicz, A. Couairon, and V. T. Tikhonchuk, Phys. Rev. Lett. **98**, 235002 (2007).
[14] K. Y. Kim, J. H. Glownia, A. J. Taylor, and G. Rodriguez, Opt. Express **15**, 4577 (2007).
[15] K. Y. Kim, A. J. Taylor, J. H. Glownia, and G. Rodriguez, Nat. Photon. **2**, 605 (2008).

[16] D. J. Cook and R. M. Hochstrasser, Opt. Lett. **25**, 1210 (2000).
[17] X. Xie, J. Dai, and X.-C. Zhang, Phys. Rev. Lett. **96**, 075005 (2006).
[18] J. Dai, X. Xie, and X.-C. Zhang, Phys. Rev. Lett. **97**, 103903 (2006).
[19] T. Löffler, F. Jacob, and H. G. Roskos, Appl. Phys. Lett. **77**, 453 (2000).
[20] T. Löffler and H. G. Roskos, J. Appl. Phys. **91**, 2611 (2002).
[21] M. Kreß, T. Löffler, M. D. Thomson, R. Dörner, H. Gimpel, K. Zrost, T. Ergler, R. Moshammer, U. Morgner, J. Ullrich, and H. G. Roskos, Nat. Phys. **2**, 327 (2006).
[22] M. Kreß, T. Löffler, S. Eden, M. Thomson, and H. G. Roskos, Opt. Lett. **29**, 1120 (2004).
[23] V. B. Gildenburg and N. V. Vvedenskii, Phys. Rev. Lett. **98**, 245002 (2007).
[24] H. Wen and A. M. Lindenberg, Phys. Rev. Lett. **103**, 023902 (2009).
[25] J. Dai, N. Karpowicz, and X.-C. Zhang, Phys. Rev. Lett. **103**, 023001 (2009).
[26] I. Babushkin, W. Kuehn, C. Köhler, S. Skupin, L. Bergé, K. Reimann, M. Woerner, J. Herrmann, and T. Elsaesser, Phys. Rev. Lett. **105**, 053903 (2010).
[27] I. Babushkin, S. Skupin, A. Husakou, C. Köhler, E. Cabrera-Granado, L. Bergé, and J. Herrmann, New J. Phys. **13**, 123029 (2011).
[28] L. Bergé, S. Skupin, C. Köhler, I. Babushkin, and J. Herrmann, Phys. Rev. Lett. **110**, 073901 (2013).
[29] A. Debayle, L. Gremillet, L. Bergé, and C. Köhler, Opt. Express **22**, 13691 (2014).
[30] D. Zhang, Z. Lü, C. Meng, X. Du, Z. Zhou, Z. Zhao, and J. Yuan, Phys. Rev. Lett. **109**, 243002 (2012).
[31] Z. Lü, D. Zhang, C. Meng, X. Du, Z. Zhou, Y. Huang, Z. Zhao, and J. Yuan, J. Phys. B **46**, 155602 (2013).
[32] Z. Zhou, D. Zhang, Z. Zhao, and J. Yuan, Phys. Rev. A **79**, 063413 (2009).
[33] A. A. Silaev and N. V. Vvedenskii, Phys. Rev. Lett. **102**, 115005 (2009).
[34] N. Karpowicz and X.-C. Zhang, Phys. Rev. Lett. **102**, 093001 (2009).
[35] L. N. Alexandrov, M. Yu Emelin, and M. Yu Ryabikin, J. Phys. B **47**, 204028 (2014).
[36] N. Dudovich, O. Smirnova, J. Levesque, Y. Mairesse, M. Y. Ivanov, D. M. Villeneuve, and P. B. Corkum, Nat. Phys. **2**, 781 (2006).
[37] J. Mauritsson, P. Johnsson, E. Gustafsson, A. L'Huillier, K. J. Schafer, and M. B. Gaarde, Phys. Rev. Lett. **97**, 013001 (2006).
[38] Y. Oishi, M. Kaku, A. Suda, F. Kannari, and K. Midorikawa, Opt. Express **14**, 7230 (2006).
[39] G. Doumy, J. H. Wheeler, C. Roedig, R. Chirla, P. Agostini, and L. F. DiMauro, Phys. Rev. Lett. **102**, 093002 (2009).
[40] J. M. Dahlström, A. L'Huillier, and J. Mauritsson, J. Phys. B **44**, 095602 (2011).
[41] J. Itatani, J. Levesque, D. Zeidler, H. Niikura, H. Pépin, J.-C. Kieffer, P. B. Corkum, and D. M. Villeneuve, Nature (London) **432**, 867 (2004).
[42] C. Vozzi, R. Torres, M. Negro, L. Brugnera, T. Siegel, C. Altucci, R. Velotta, F. Frassetto, L. Poletto, P. Villoresi, S. De Silvestri, S. Stagira, and J. P. Marangos, Appl. Phys. Lett. **97**, 241103 (2010).
[43] M. V. Ammosov, N. B. Delone, and V. P. Krainov, Sov. Phys. JETP **64**, 1191 (1986).
[44] E. Priori, G. Cerullo, M. Nisoli, S. Stagira, S. De Silvestri, P. Villoresi, L. Poletto, P. Ceccherini, C. Altucci, R. Bruzzese, and C. de Lisio, Phys. Rev. A **61**, 063801 (2000).
[45] X. M. Tong and C. D. Lin, J. Phys. B **38**, 2593 (2005).
[46] A. A. Silaev, M. Y. Ryabikin, and N. V. Vvedenskii, Phys. Rev. A **82**, 033416 (2010).
[47] N. V. Vvedenskii, A. I. Korytin, V. A. Kostin, A. A. Murzanev, A. A. Silaev, and A. N. Stepanov, Phys. Rev. Lett. **112**, 055004 (2014).
[48] M. Clerici, M. Peccianti, B. E. Schmidt, L. Caspani, M. Shalaby, M. Giguère, A. Lotti, A. Couairon, F. M. C. Légaré, T. Ozaki, D. Faccio, and R. Morandotti, Phys. Rev. Lett. **110**, 253901 (2013).
[49] Y. S. You, T. I. Oh, A. B. Fallahkhair, and K. Y. Kim, Phys. Rev. A **87**, 035401 (2013).
[50] J. Wu, Y. Tong, M. Li, H. Pan, and H. Zeng, Phys. Rev. A **82**, 053416 (2010).
[51] M. Lein, N. Hay, R. Velotta, J. P. Marangos, and P. L. Knight, Phys. Rev. A **66**, 023805 (2002).
[52] Y. Mairesse, A. de Bohan, L. J. Frasinski, H. Merdji, L. C. Dinu, P. Monchicourt, P. Breger, M. Kovacev, R. Taïeb, B. Carré, H. G. Muller, P. Agostini, and P. Salière, Science **302**, 1540 (2003).